15th IFK
Proc. of the 15th International Fluid Power Conference <Symposium/Conference>
<DOI>

Percolation Analysis of Reciprocating Sealing Surfaces Based on the Statistical Evolution of HPD and PSD Induced by Wear

Jiehao Wang[1], Jing Li[2], Wei Shen[1], Katharina Schmitz[3]

1. Department of Mechatronics Engineering, University of Shanghai for Science and Technology; 2. School of Mechanical Engineering, Tongji University; 3. Institute for Fluid Power Drives and Systems (ifas), RWTH Aachen University

Abstract.

The reciprocating seal exhibits significantly different wear behaviours and surface damage patterns under various friction and operating conditions. Precisely describing the topography characteristics of the worn surface is of great significance for the analysis of oil flow and the study of the leakage mechanism. The high probability density (HPD) and the power spectral density (PSD) are commonly used for reconstructing the surface topography. It is particularly necessary to study the evolution laws of HPD and PSD during the wear process to reconstruct worn surface. This study is based on the polymer-steel reciprocating friction experiments and analyses the changes in HPD and PSD characteristics of the PTFE worn surface under different temperatures. A three-dimensional oil percolation simulation model is established to reflect the flow characteristics of the oil fluid on the sealing contact surface. Based on the actual worn surface, the evolution laws of the surface topography under different wear mechanisms are revealed. On this basis, a numerical algorithm based on HPD and PSD is proposed to realize the predictive reconstruction of the worn surface topography. The reconstructed surface can be applied to the oil percolation simulation to explore the influence of surface topography evolution on sealing performance and leakage characteristics. The research results provide a theoretical basis for understanding the wear mechanism of polymer, predicting the sealing life, and revealing the failure mechanism.

Keywords. Reciprocating seal, percolation analysis, surface reconstruction, polymer wear, oil leakage

1. INTRODUCTION

Hydraulic systems are widely used in key fields such as aerospace, shipbuilding, and high-end equipment manufacturing due to their high-power density, rapid response, and excellent reliability [1]. In hydraulic systems, the actuator is the core actuator component, and its performance and stability play a decisive role in the overall operation of the system. Among them, the reciprocating seal mechanism is a key functional link in the actuator. The stability, reliability, and service life of its sealing performance are directly related to the working efficiency and operational safety of the actuator [2]. The failure of the seal will not only significantly reduce the transmission efficiency of the hydraulic system but also increase maintenance costs [3].

Reciprocating seal structures exhibit distinct multiscale coupling characteristics, integrating the functions of both a sealing pair and a friction pair. Their sealing interfaces often experience a complex mixed lubrication state. Although a fluid oil film effectively separates some contact areas, the film thickness is insufficient to completely cover the microscopic topography of the sealing surface, leading to unavoidable direct contact between surface roughness peaks [4]. Mechanical contact between these submicron-scale roughness peaks not only disrupts the continuity of the oil film but can also trigger complex wear mechanisms within the contact area, including localized stress concentration, severe plastic deformation, adhesive wear, and material delamination [5].

Due to the complex and variable working conditions of sealing pairs, traditional testing methods have difficulty accurately capturing their contact state and stress evolution. Current research on the failure modes and life prediction of aerospace actuator seals is primarily based on material fatigue damage criteria. However, the microscopic topography characteristics of the contact surface are crucial for revealing the mixed lubrication behaviour, as well as the friction and wear mechanisms during service [6, 7]. As the actuator continues to operate, the contact surface topography evolves, and the lubrication state also changes accordingly. The interaction between the two ultimately drives the degradation of seal performance and wear failure. Therefore, obtaining the characteristics of surface topography evolution during service and conducting an in-depth analysis of the bidirectional coupling mechanism between lubrication and wear are key to revealing the essential mechanism of seal failure [8].

To understand the contact behaviour of rough surfaces, Persson et al. proposed a multiscale contact theory model for the elastic-plastic contact behaviour of random rough surfaces [9, 10]. This model assumes that the material exhibits an elastic response below the yield stress and undergoes plastic flow above it. On this basis, a linear relationship between the actual contact area and the normal load is derived. In the absence of plastic deformation, the actual contact area of a rough surface with self-affine fractal characteristics shows a power-law relationship with the lateral scale of the nominal contact area. This model emphasizes the surface power spectrum density (PSD) as the core parameter to characterize the multiscale characteristics of the rough surface and establish a quantitative relationship between it and macroscopic properties such as contact area, pressure distribution, and friction [11, 12].

Based on this contact theory, Persson et.al further expanded their research, introducing a coupling model of percolation theory and contact mechanics to explore the leakage behaviour and microscopic mechanism of seals under static and dynamic conditions [13]. Through multi-scale analysis of the power spectrum (PS) of rough surfaces, theoretical and numerical simulations showed that the formation and evolution of percolation channels are the key driving factors for leakage at the sealing interface. On this basis, Lorenz et al. developed a leakage prediction method based on the effective medium theory (EMT), treating the oil flow at the sealing interface as propagating in multiple independent microchannels, and combined the surface power spectrum to analyze the statistical evolution of the seal contact area and gap height [14]. Bottiglione et al. further integrated the seal geometry, applied load, and surface roughness parameters to construct a comprehensive numerical model that can simulate contact randomness and predict leakage rate [15]. Scaraggi et al. proposed a numerical method to study the oil extrusion behaviour between soft elastic bodies and random rough rigid surfaces based on the transient mixed elastohydrodynamic lubrication theory [16].

Peng et al. analysed the differences between the multi-asperity model and the magnification-based percolation model in predicting sealing performance [17]. The study focused on the numerical prediction of gas leakage in metal sealing structures. By comparing the simulation results with the experimental data, it was found that the magnification-based percolation model performed better in leakage prediction accuracy. The model can directly characterize the microscopic topography characteristics of the sealing contact surface and analyze the spatial distribution of the contact and gap areas based on the PSD function, thereby revealing the generation mechanism of the oil percolation channel. Therefore, the model shows advantages in evaluating the influence of surface topography on local leakage behaviour.

However, the percolation model still has certain limitations:

- Current percolation calculations are mainly based on the PSD function, making it difficult to effectively couple the effects of seal load, temperature, and dynamic wear under real working conditions;
- Existing percolation theories use one-dimensional (1D) PSD functions to describe surface roughness distribution, which cannot capture the anisotropic characteristics of the worn surface.

To address the limitations of existing percolation models in coupling to actual operating conditions and characterizing surface anisotropy, this paper proposes a method for simulating oil percolation based on numerically reconstructed surface topography. This method conducts seal wear tests under typical operating conditions to obtain actual act contact surface topography data at different service stages. Based on this data, the worn surface is numerically reconstructed, and parameter extraction is performed. Furthermore, the statistical distribution and evolution of characteristic wear topography parameters are analysed, and a correlation model between wear topography and percolation characteristics is constructed, which allows for quantitative prediction and mechanistic understanding of oil percolation behaviour on worn sealing surfaces.

2. WEAR TEST

2.1. Test method

The RTEC MFT-5000 multi-functional wear testing machine was used to conduct wear tests on the commonly used material PTFE (polytetrafluoroethylene) for the wear ring. To investigate the wear characteristics of the PTFE specimens under high-temperature conditions, the specimens were heated for 15 minutes before the wear test to ensure that the material of the specimens reached thermal stability. An infrared thermal imager was used to perform real-time imaging and temperature measurement of the PTFE specimens. The specific test parameters are shown in Table 2.1.

Table 2.1 PTFE material wear test parameters

Parameters	Value
Test material	PTFE
Wear type	Ball-on-disk
Roughness of specimen	3-4μm
Grinding piece	Cr15 ball with a diameter of 4 mm
Single stroke	2mm
Frequency	3Hz
Normal load	10N
Test time	10 mins
Test temperature	20, 60°C

The worn surface can be observed and measured using two methods. A digital microscope is employed for micro-imaging of the worn surface, capturing the details of wear marks, analysing surface damage modes, and identifying different wear mechanisms. A laser confocal profilometer is used to acquire data on wear tracks and local surface topography. This data is then imported into Mountains Map software for analysis to obtain high-precision measurements of wear depth and surface topographic features. A 3D surface topography model of the worn area is reconstructed, providing data support for further analysis of the worn surface characteristics. The equipment used for wear tests is shown in Figure2.1.

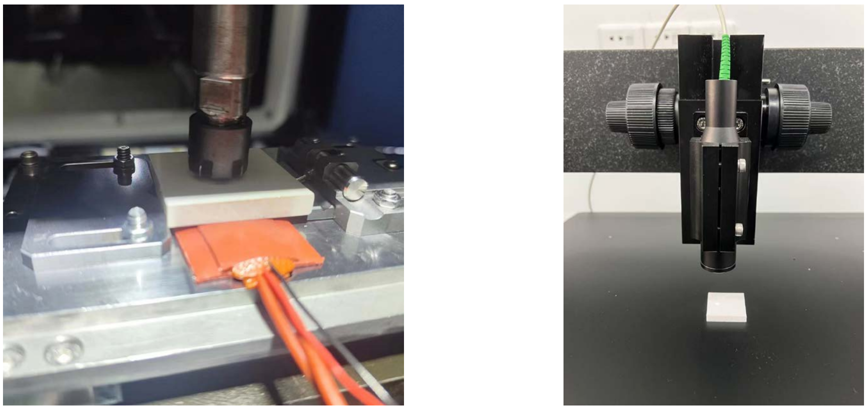

(a) MFT-5000 wear testing machine (b) Laser confocal profilometer

Figure 2.1. Wear test equipment

2.2. *Test results*

Figure2.2 shows the worn surface of PTFE at different temperatures and times. At 20°C, the PTFE surface exhibits typical scratch-like abrasive wear characteristics. The wear mechanism at this point is primarily driven by the cutting action of hard particles, resulting in a plowing effect. When the temperature rises to 60°C, the surface material starts to peel off, and localized depressions appear, predominantly exhibiting a ridge-like adhesive wear topography. The interfacial adhesion of the material is enhanced under high temperature conditions, making adhesive wear the dominant wear mechanism.

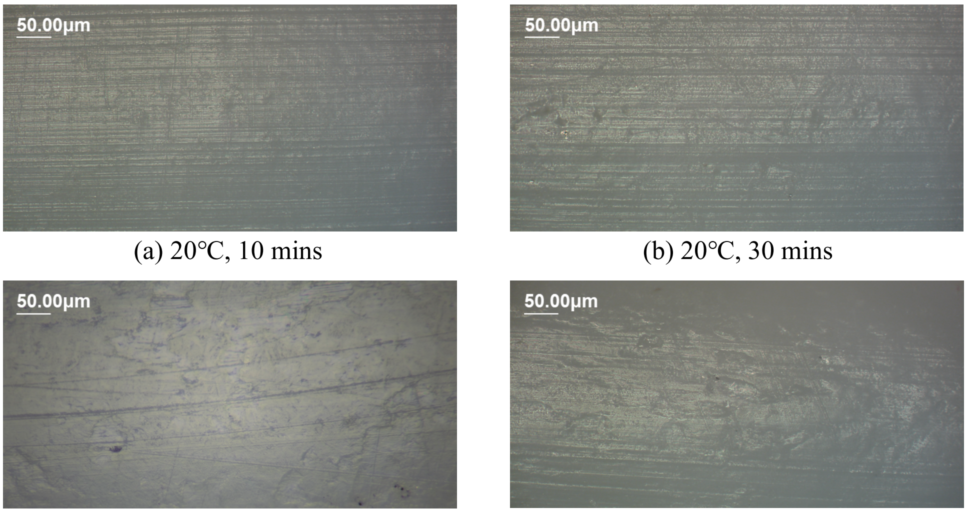

(a) 20℃, 10 mins (b) 20℃, 30 mins

(c) 60℃, 10 mins (d) 60℃, 30 mins

Figure 2.2. Worn surfaces of PTFE under different temperatures and durations

The variation of PTFE friction coefficient with wear time at different temperatures is shown in Figure2.3. From a wear mechanism perspective, abrasive wear occurs when hard abrasive particles embed themselves in the PTFE surface and scratch across it, creating a cutting or plowing effect. Adhesive wear primarily occurs when localized adhesion nodes form between the rough peaks of the two contacting surfaces, leading to material removal due to tearing caused by relative motion. At room temperature, PTFE is rigid and elastic, resulting in a small actual contact area and high local pressure, which in turn generates high interfacial shear forces. However, at high temperatures, the softening of PTFE reduces adhesion strength, reducing the adhesion between adhesion nodes.

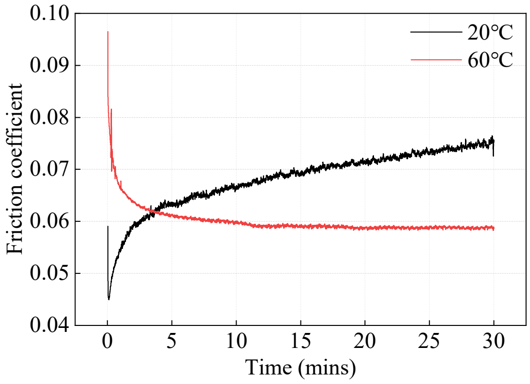

Figure 2.3. Friction coefficient variation of PTFE

The wear rate is calculated by scanning the average wear depth on the worn surface. The wear rates at 20°C and 60°C are $5.86 \times 10^{-5} mm^3/Nm$ and $9.08 \times 10^{-5} mm^3/Nm$, respectively. Notably, the wear volume of PTFE does not show a positive correlation with the friction coefficient.

2.3. *Worn surface topography*

With a surface sampling accuracy of 0.7 μm, a 200×200 node area in the centre of the worn surface is selected for quantitative analysis of surface topography. Typical surface topography at 20°C and 60°C are shown in Figure2.4. At 20°C, the worn surface exhibits anisotropic characteristics, with wear scars exhibiting clear directionality. Wear primarily occurs in a specific direction. At 60°C, the worn surface exhibits isotropic characteristics, caused by the formation of uniform and discrete adhesive nodes on the surface.

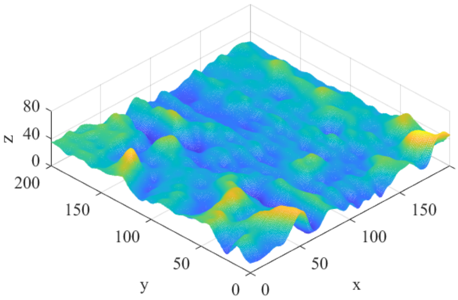

(a) 20°C, 30 mins

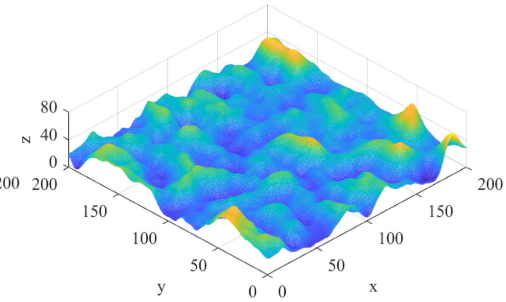

(b) 60°C, 30 mins

Figure 2.4. Localized worn surface topography

1D PSD can be used to characterize the topography characteristics of rough surfaces, reveal microscopic changes in a single direction of the worn surface. By screening all frequency points projected to the specified direction angle θ at the spatial frequency q, and performing normalization processing, the 1D average PSD function is

$$C_{1D}(q,\theta)=\frac{\int_{-\infty}^{\infty}\int_{-\infty}^{\infty}C_{2D}(q_x,q_y)\delta_d(q-q_\theta)dq_x dq_y}{\int_{-\infty}^{\infty}\int_{-\infty}^{\infty}\delta(q-q_\theta)dq_x dq_y} \tag{2.1}$$

where δ is the Dirac function; q_θ is the specified direction projection length.

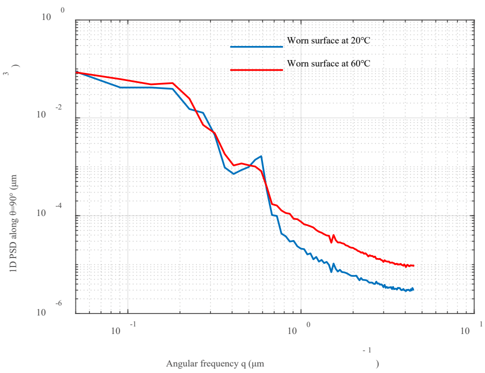

(a) 1D PSD along $\theta = 90°$

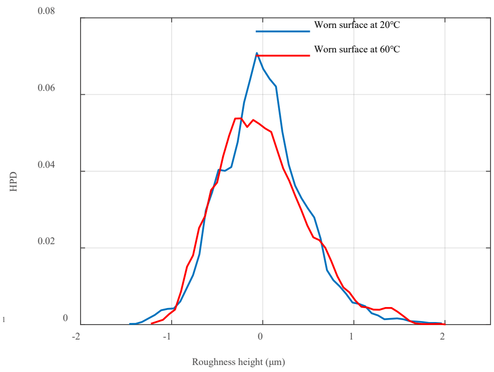

(b) HPD

Figure 2.5. Worn surface statistical characteristics

Figure2.5 shows the 1D PSD along the friction direction (defined as $\theta = 90°$) and the height probability distribution (HPD) of roughness at 20℃ and 60℃. The 1D PSD variation of the worn surface reflects the transition between its anisotropic and isotropic characteristics. At 20°C, the worn surface exhibits strong anisotropy, with slight surface fluctuations along the friction direction, resulting in a low PSD of the high-frequency domain. At 60°C, the worn surface tends to be isotropic, with the energy distribution of the surface topography being relatively uniform in different directions, resulting in a higher overall PSD. The result is consistent with the observation of the worn surface topography, indicating that the wear mechanism significantly impacts the worn surface structure and its spectral characteristics.

The root mean square (RMS) roughness increases with temperature. The softening of PTFE at high temperatures intensifies wear, resulting in a rougher worn surface. The HPD of worn surfaces at both temperatures exhibits positive skewness, with numerous peaks formed by material spalling, exhibiting an asymmetric distribution. Higher temperatures exacerbate the unevenness of the worn surface height.

3. PREDICTIVE RECONSTRUCTION OF WORN SURFACE

3.1. Surface reconstruction

The surface topography reconstruction method proposed by Pérez-Ràfols is adopted, in which the PS and HPD are used as inputs to generate random surfaces that simultaneously satisfy both statistical characteristics [18]. First, two random rough surfaces with height sequences Z_h^0 and Z_s^0 are generated. The surface Z_h^0 has a height distribution consistent with the given HPD but does not meet the target PS requirement, whereas surface Z_s^0 satisfies the desired PS but deviates from the target HPD.

Both surfaces are then subjected to two-dimensional Fourier transforms, yielding their frequency-domain counterparts $\hat{Z}_h^0$ and $\hat{Z}_s^0$. Then, an iterative correction process is applied to gradually adjust the surfaces so that they meet both target distributions. This process alternates between two main steps:

- Adjusting the surface in the frequency domain to match the target PS.
- Correcting the surface in the spatial domain to match the target HPD.

Through iteration, both the PS and HPD of the reconstructed surface converge toward the specified target distributions, thereby realizing a random surface generation method that simultaneously satisfies the prescribed PS and HPD. The PS of Z_h^i is corrected and the Z_s^{i+1} that satisfies the target PS is characterized using the spectral representation method, that is

$$Z_s^{i+1} = FFT^{-1}\left[\sqrt{S} \times exp\left(i\phi_h^i\right)\right] \tag{3.1}$$

where, ϕ_h^i represents the phase in the frequency domain, which can be expressed in terms of the real and imaginary parts of $\hat{Z}_h^i$ obtained from the previous iteration as follows:

$$\phi_h^i = tan^{-1}\left(\frac{Im\left(\hat{Z}_h^i\right)}{Re\left(\hat{Z}_h^i\right)}\right) \tag{3.2}$$

At this stage, the PS of Z_s^{i+1} satisfies the target, but the HPD does not meet the requirements. By mapping the height distribution of Z_h^{I} onto Z_s^{i+1}, a new iteration of Z_h^{i+1}

that satisfies the target HPD can be obtained. Three types of errors are introduced to evaluate how well the generated surface matches the target surface in terms of PS and HPD [19].

i. Height probability distribution error err_h — quantifies the deviation between the actual height distribution of the generated surface and the target height distribution:

$$err_h = \sum_{i=1}^{N_b} |n_{ih} - n_{is}| \cdot \omega_b \tag{3.3}$$

where n_{ih} and n_{is} represent the frequency of occurrence of surface heights within a given height interval in the histograms of the target and generated surfaces, respectively; N_b is the total number of height intervals, and ω_b is the interval width.

ii. Power spectrum error (nonzero region) err_s — reflects the discrepancy between the nonzero power spectrum values of the generated surface and those of the target surface:

$$err_s = \sqrt{\frac{1}{N_s} \sum_{q_i=q_0}^{q_1} \left(\frac{|\hat{Z}_s(q_i)| - |\hat{Z}_h(q_i)|}{|\hat{Z}_s(q_i)|} \right)^2} \tag{3.4}$$

where $\hat{Z}_s(q_i)$ and $\hat{Z}_h(q_i)$ are the power spectrum values of the target surfaces at spatial frequency q_i; N_s denotes the number of nonzero spatial frequencies in the target power spectrum; q_0 and q_1 are the lower and upper cutoff spatial frequencies.

iii. Power spectrum error (zero region) err_{s0} — characterizes the performance of the generated surface in the frequency range where the target power spectrum is zero:

$$err_{s0} = \frac{\sqrt{\frac{1}{N_{s0}} \sum_{q_i<q_0 | q_i>q_1} |\hat{Z}_h(q_i)|^2}}{\frac{1}{N_s} \sum_{q_0 \le q_i \le q_1} |\hat{Z}_s(q_i)|} \tag{3.5}$$

where N_{s0} denotes the number of spatial frequencies for which the target power spectrum is zero. The iterative process continues until all three errors fall below the specified thresholds, at which point the generated surface is considered to meet the target requirements.

3.2. Topography characterization

(1) Power spectral density

The power spectral density ratio function corresponding to the 1D PSD frequency point $q_{1D}^i \in S_q$ is expressed as follows:

$$R_{1D}(q_{1D}^i) = \begin{cases} 1, & q_{1D}^i < q_s \\ \alpha_{psd}, & q_{1D}^i \ge q_s \end{cases} \tag{3.6}$$

where, α_{psd} is the power-spectrum scaling coefficient, and q_s is the adjustment frequency threshold. Using an interpolation function, the ratio function $R_{1D}(q_{1D}^i)$, which is discretely defined on the 1D PSD, is mapped into the two-dimensional (2D) frequency domain to obtain for each point $q_{2D}^{k,l}$ in the frequency coordinate system, its scaling factor [20]:

$$R_{2D}(q_{2D}^{k,l}) = R_{1D}(q_{1D}^i) + \frac{R_{1D}(q_{1D}^{i+1}) - R_{1D}(q_{1D}^i)}{q_{1D}^{i+1} - q_{1D}^i} \cdot (q_{2D}^{k,l} - q_{1D}^i) \tag{3.7}$$

where R_{2D} is the 2D PSD ratio function, and $q_{2D}^{k,l} \in [q_{1D}^{i}, q_{1D}^{i+1}]$. As worn surfaces typically exhibit pronounced anisotropy, the adjustment in the frequency domain is applied only to the frequency components along the target direction. Let $\tilde{\theta}$ denote the direction angle of an arbitrary frequency in the frequency domain, θ is the target direction, and θ_t is the directional tolerance. The directional mask matrix for the spatial frequency $q_{2D}^{k,l}$ in the 2D frequency domain is

$$Mar(q_x^k, q_y^l) = \begin{cases} 1, \left|\tilde{\theta}(q_x^k, q_y^l) - \theta\right| < \theta_t \\ 0, \left|\tilde{\theta}(q_x^k, q_y^l) - \theta\right| \geq \theta_t \end{cases} \tag{3.8}$$

The adjusted two-dimensional power spectral density function is

$$C_{2D}{}'(q_x^k, q_y^l) = \begin{cases} R_{2D}(q_{2D}^{k,l}) \cdot C_{2D}(q_x^k, q_y^l), & Mar(q_x^k, q_y^l) = 1 \\ C_{2D}(q_x^k, q_y^l), & Mar(q_x^k, q_y^l) = 0 \end{cases} \tag{3.9}$$

(2) Height probability density

Johnson transform is a distribution transformation method based on data statistical analysis, which can be used to convert between Gaussian sequences and non-Gaussian sequences [21]. The skewness and kurtosis of the input and output height sequences have the following relationship [22]:

$$Sk_0 = \frac{\left(\sum_{r=0}^{M-1} \sum_{s=0}^{N-1} f(r,s)^2\right)^{\frac{3}{2}}}{\sum_{r=0}^{M-1} \sum_{s=0}^{N-1} f(r,s)^3} Sk_\eta \tag{3.10}$$

$$Ku_0 = \frac{\left(\sum_{r=0}^{M-1} \sum_{s=0}^{N-1} f(r,s)^2\right)^2 Ku_\eta - 6 \sum_{r=0}^{M-2} \sum_{p=r+1}^{M-1} \sum_{s=0}^{N-2} \sum_{q=s+1}^{N-1} f(r,s)^2 f(p,q)^2}{\sum_{r=0}^{M-1} \sum_{s=0}^{N-1} f(r,s)^4} \tag{3.11}$$

where Sk_0 and Ku_0 are the input skewness and kurtosis, and Sk_η and Ku_η are the given skewness and kurtosis. r, s, p, q is the index of the coordinate in space. The surface topography is regarded as a random process. By adjusting the power spectrum density and probability distribution characteristics, the generated surface topography has a specific skewness, kurtosis and spatial correlation. The autocorrelation function is a mathematical tool used to describe the correlation of random signals, often used in roughness modelling. The exponential form is

$$R(x, y) = S_q^2 \exp\left\{-2.3 \left[(x/\beta_x)^2 + (y/\beta_y)^2\right]^{1/2}\right\} \tag{3.12}$$

where β_x and β_y are the autocorrelation lengths. By performing Fourier transform on the autocorrelation function, the output roughness height power spectral density function can be obtained:

$$S(k, l) = \frac{1}{MN} \sum_{r=0}^{M-1} \sum_{s=0}^{N-1} R(r, s) \exp\left(-\frac{j2\pi kr}{M}\right) \exp\left(-\frac{j2\pi ls}{N}\right) \tag{3.13}$$

where k, l is the frequency domain index. The two-dimensional digital filter function $f(r,s)$ can be obtained through the power spectrum density function:

$$f(r,s) = \frac{1}{MN}\sum_{r=0}^{M-1}\sum_{s=0}^{N-1}\sqrt{S(k,l)}\exp\left(-\frac{j2\pi kr}{M}\right)\exp\left(-\frac{j2\pi ls}{N}\right) \qquad (3.14)$$

3.3. Predictive reconstruction

Numerical reconstruction of the worn surface relies on the PSD and HPD obtained from experiments as statistical characteristic parameters. However, due to limitations in the number of test surfaces and the scope of surface topography acquisition, it is difficult for the experimental worn surfaces to cover all possible topography characteristics. By adjusting the PSD and HPD extracted from existing test data, a reconstruction process independent of the specific measured surface can be achieved. It can be used to simulate and predict the topography of worn surfaces with arbitrary characteristics. Furthermore, the worn surface topography can be predictive based on operating conditions to simulate oil percolation. The predictive reconstruction process of the worn surface topography is shown in Figure3.1.

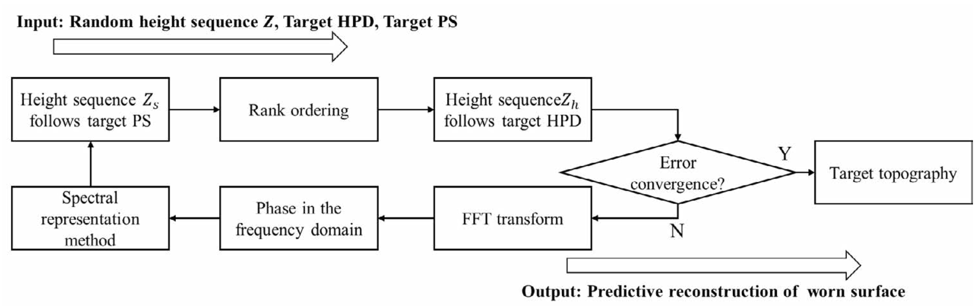

Figure 3.1. Flowchart for predictive reconstructed worn surface topography

To verify the effectiveness of the predictive reconstruction method, the worn surface at 20°C shown in Figure2.4 (a) is chosen as the research object. $\alpha_{psd} = 1.8$, $q_s = 0.6$ and $\theta_t = \pm 5°$ are selected to adjust its PSD. The results are shown in Figure3.2.

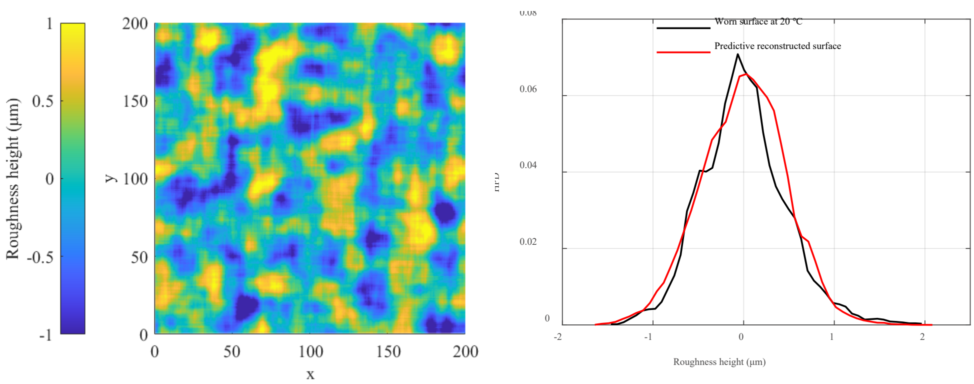

(a) Reconstructed surface (b) HPD

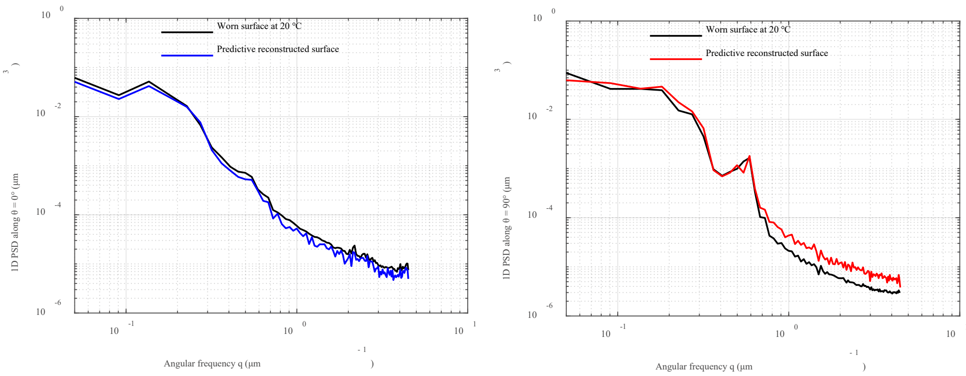

(c) 1D PSD along $\theta = 0°$ (d) 1D PSD along $\theta = 90°$

Figure 3.2. Predictive reconstructed surface and its characteristics

Define $\theta = 90°$ as the seal's axial direction, i.e., the direction of reciprocating friction, and $\theta = 0°$ as the seal's circumferential direction, perpendicular to the reciprocating motion. By comparing the 1D PSD in these two directions, the anisotropic characteristics variation of the surface topography can be reflected.

The 1D PSD of the original worn surface in the high-frequency region of the friction direction is significantly lower than that in other directions, indicating that the surface exhibits significant anisotropy. During the prediction and reconstruction process, the 1D PSD in the high-frequency region is appropriately amplified to compensate for the surface anisotropy. The anisotropy of the predictive and reconstructed surface is weakened, tending towards an isotropic state, while the HPD of the roughness remains unchanged. The 1D PSD in the $\theta = 0°$ direction remains essentially the same before and after reconstruction. The surface energy increases in the $\theta = 90°$ direction and when $q > 0.6$, demonstrating that this method effectively adjusts the high-frequency characteristics in the target direction without affecting the roughness characteristics in other directions.

4. OIL PERCOLATION ANALYSIS

4.1. Actual worn surface

The paper adopts the oil percolation simulation method proposed in Ref [23] to conduct three-dimensional simulations of the percolation behaviour of worn surfaces obtained from tests at 20°C and 60°C. By extracting oil film thickness distribution data from the seal contact surface, an oil channel structure model of the oil percolation can be constructed, enabling the analysis of oil flow behaviour within the percolation channel. Figure4.1 shows the flow velocity distribution within the oil percolation channel on the sealing surface at different temperatures.

The oil leakage rates on the worn surface at 20°C and 60°C are $2.81 \times 10^{-5} cm^3/s$ and $3.62 \times 10^{-5} cm^3/s$. PTFE produces significant shear deformation and stress dispersion due to its excellent energy dissipation capabilities. This process suppresses the ability of abrasive particles to create deep scratches on the surface during ploughing effect. In contrast, adhesive wear primarily results from localized adhesion between the materials at the contacting surfaces. Under reciprocating shear loads, adhesive nodes fracture and material delamination occur, and their formation is closely related to the adhesive strength of the contact interface. At high temperatures (e.g., 60°C), thermal softening of the material enhances adhesive strength, making it more likely to form deeper wear scars.

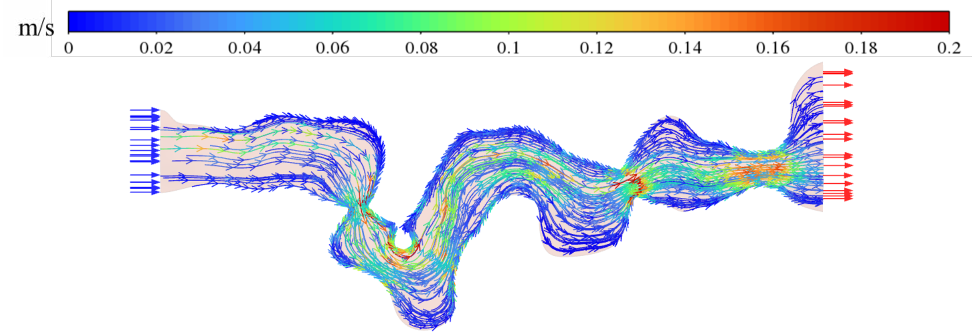

(a) Actual worn surfaces at 20°C

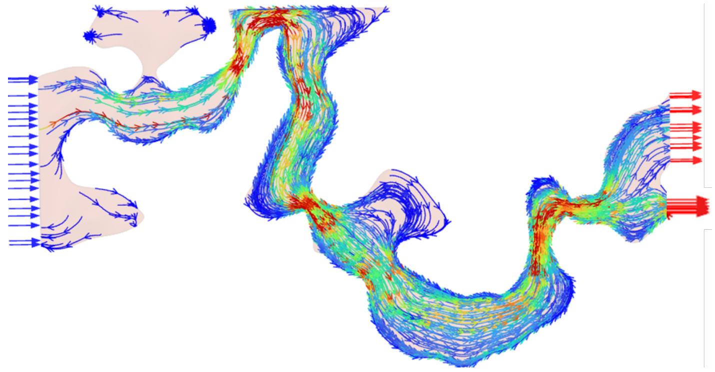

(b) Actual worn surfaces at 60°C

Figure 4.1. Oil percolation characteristics of actual worn surfaces

Therefore, the worn surface at 60°C is more susceptible to enhanced adhesive wear than that at 20°C. The oil flow channels exhibit variation in cross-sectional geometry, particularly in the critical constriction, where a larger channel area and higher oil flow rate are observed. This phenomenon indicates that high-temperature operating conditions not only alter the dominant wear mechanism but also significantly affect the lubrication and flow properties of the sealing surface, impacting the stability of sealing performance.

4.2. Predictive reconstructed worn surface

To investigate the influence of the reconstructed worn surfaces on the analysis results of percolation characteristics, analyses are conducted on these surfaces at 20°C and 60°C. The results are then compared with those from the test worn surfaces. The reconstructed worn surfaces for percolation analysis are shown in Figure4.2. The RMS roughness of the reconstructed surfaces is consistent with that of the actual worn surfaces. This consistency eliminates the interference of roughness differences on the percolation behaviour, thereby more accurately evaluating the influence of surface reconstruction on the percolation channel structure, velocity distribution, and other related factors.

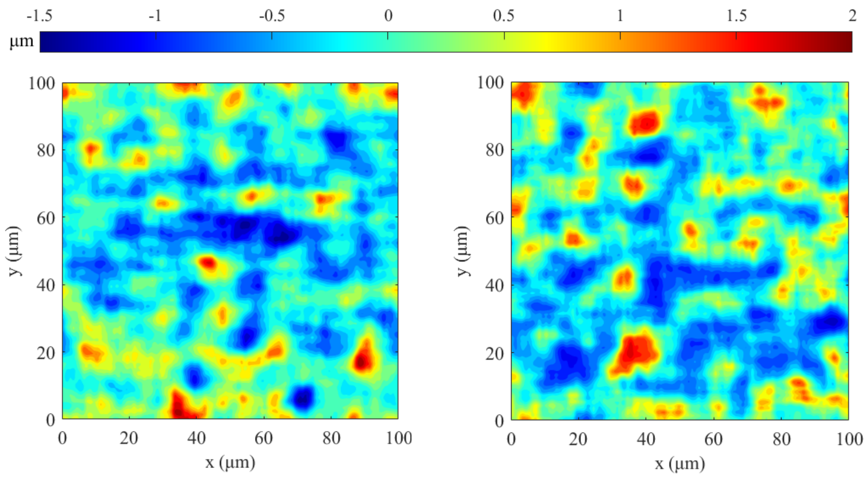

(a) Reconstructed surface at 20°C (b) Reconstructed surface at 60°C

Figure 4.2. Predictive reconstructed worn surfaces for percolation analysis

Figure4.3 shows the oil percolation characteristics on the predictive reconstructed worn surfaces at different temperatures.

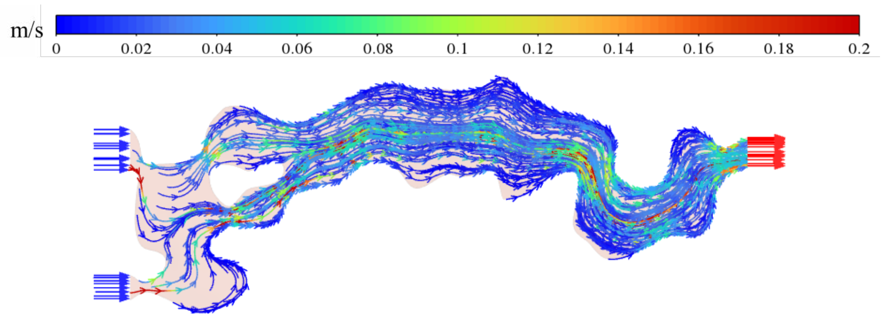

(a) Predictive reconstructed worn surface at 20°C

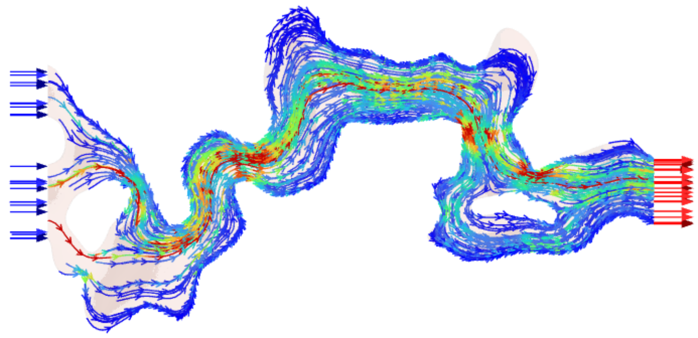

(b) Predictive reconstructed worn surface at 60°C

Figure 4.3. Oil percolation characteristics of predictive reconstructed worn surfaces

At 20°C, a wide but shallow percolation channel is formed along the reciprocating motion direction on the reconstructed worn surface, and the oil flow velocity is relatively low. At

60°C, the width of the percolation channel at the critical constriction is narrower, but due to the increase in the wear depth of the sealing surface, a larger effective flow area is formed, and the local maximum flow velocity reached 0.181 m/s. Compared to the width, the height of the percolation channel directly determines the oil film thickness and has a greater impact on the overall flow capacity of the channel.

The numerical calculation of the net leakage rate of oil on the reconstructed worn surface is conducted, and it is compared with the analysis results of the leakage rate on the corresponding actual worn surface, as shown in Figure4.4.

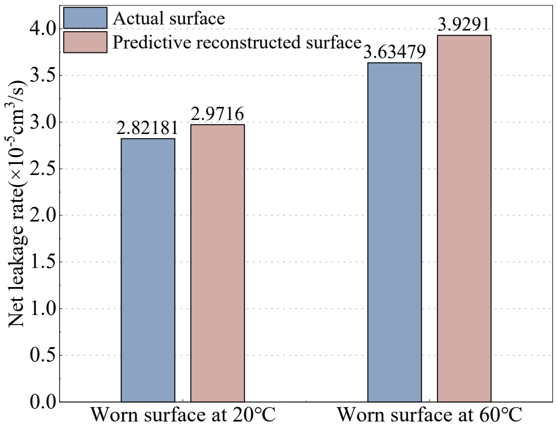

Figure 4.4. Comparison of net leakage rate results

Since the reconstructed surface maintains the same topography characteristic parameters as the actual surface, such as PSD, HPD, RMS roughness, etc., both show similar leakage characteristics. The leakage rate of the reconstructed surface is slightly higher than that of the actual surface. The error arises from the differences in the topography structure arrangement and topological form of the reconstructed surface compared to the actual surface. The topography affects the contact state and percolation channels, resulting in different leakage rates. However, the error is relatively small, and the reconstructed surface can more accurately reflect the change trend of the leakage rate under different temperatures. It still has good reliability in predicting oil leakage.

5. CONCLUSION

As the wear temperature increases, the surface damage pattern changes from continuous scratches along the reciprocating direction to discrete, localized adhesive failure nodes, indicating a shift from abrasive to adhesive wear. Material exfoliation depressions, resulting from shear-adhesive nodes, begin to appear on the worn surface. During the abrasive wear-dominated phase, the friction coefficient is high. In contrast, during the adhesive wear-dominated phase, the softening of the PTFE surface reduces shear strength and the friction coefficient. A method for predicting and reconstructing worn surface topography is developed. This method reconstructs a surface with identical PSD and HPD statistical characteristics from experimentally derived worn surface topography.

Furthermore, the anisotropic characteristics of the original surface are modified by adjusting its 1D PSD along a single direction. The HPD of the surface roughness can be modified using a Johnson transform. Comparison of oil percolation analysis results between the original and predictive reconstructed surfaces reveals that, due to differences in morphological arrangement and topology, the leakage rate calculations exhibit minimal error, accurately reflecting the leakage rate trends of the worn surfaces at different temperatures. At room temperature, grooves created by abrasive wear easily form percolation channels that penetrate the sealing surface. However, due to the shallow wear depth, leakage is low. At high temperatures, adhesive failure nodes cause significant material removal, forming large cross-sectional percolation channels that increase overall flow capacity and leakage.

6. References

[1] G. K. Nikas, ‘Eighty years of research on hydraulic reciprocating seals: Review of tribological studies and related topics since the 1930s’, Proc. Inst. Mech. Eng., Part J, vol. 224, no. 1, pp. 1–23, Jan. 2010. doi: https://doi.org/10.1243/13506501jet607

[2] B. Wang, X. Meng, X. Peng, and Y. Chen, ‘Experimental investigations on the effect of rod surface roughness on lubrication characteristics of a hydraulic O-ring seal’, Tribol. Int., vol. 156, pp. 106791–106791, Apr. 2021. doi: https://doi.org/10.1016/j.triboint.2020.106791

[3] D. Liu, S. Wang, and C. Zhang, ‘A multiscale wear simulation method for rotary lip seal under mixed lubricating conditions’, Tribol. Int., vol. 121, pp. 190–203, Jan. 2018. doi: https://doi.org/10.1016/j.triboint.2018.01.007

[4] D. Zhu and Y.-Z. Hu, ‘A computer program package for the prediction of EHL and mixed lubrication characteristics, friction, subsurface stresses and flash temperatures based on measured 3-D surface roughness,” Tribol. Tran., vol. 44, no. 3, pp. 383–390, Jan. 2001. doi: https://doi.org/10.1080/10402000108982471

[5] A. P. Nyemeck, Noël Brunetiere, and B. Tournerie, ‘A mixed thermoelastohydrodynamic lubrication analysis of mechanical face seals by a multiscale approach’, Tribol. Trans., vol. 58, no. 5, pp. 836–848, Mar. 2015. doi: https://doi.org/10.1080/10402004.2015.1023407

[6] G. K. Nikas and R. S. Sayles, ‘Study of leakage and friction of flexible seals for steady motion via a numerical approximation method’, Tribol. Int., vol. 39, no. 9, pp. 921–936, Sep. 2006. doi: https://doi.org/10.1016/j.triboint.2005.09.003

[7] Y. Z. Hu and K. Tonder, ‘Simulation of 3-D random rough surface by 2-D digital filter and fourier analysis’, Int. J. Mach. Tools. Manuf., vol. 32, no. 1–2, pp. 83–90, Feb. 1992. doi: https://doi.org/10.1016/0890-6955(92)90064-N

[8] T. Yin, J. Fu, D. Wei, Z. Xie, E. Zhang, and B. Zhao, ‘Thermal contact of roughness macro and micro model to reveal seal leakage mechanism under mixed lubrication’, Tribol. Int., vol. 191, p. 109176, Mar. 2024. doi: https://doi.org/10.1016/j.triboint.2023.109176

[9] B. N. J. Persson, ‘Elastoplastic Contact between Randomly Rough Surfaces’, Phys. Rev. Lett., vol. 87, no. 11, Aug. 2001. doi: https://doi.org/10.1103/physrevlett.87.116101

[10] B. N. J. Persson, ‘Theory of rubber friction and contact mechanics’, J. Chem. Phys., vol. 115, no. 8, pp. 3840–3861, Aug. 2001. doi: https://doi.org/10.1063/1.1388626

[11] B. N. J. Persson, ‘Contact mechanics for randomly rough surfaces’, Surf. Sci. Rep., vol. 61, no. 4, pp. 201–227, Jun. 2006. doi: https://doi.org/10.1016/j.surfrep.2006.04.001

[12] C. Yang and B. N. J. Persson, ‘Contact mechanics: contact area and interfacial separation from small contact to full contact’, J. Phys.: Condens. Matter, vol. 20, no. 21, p. 215214, Apr. 2008. doi: https://doi.org/10.1088/0953-8984/20/21/215214

[13] B. N. J. Persson and C. Yang, ‘Theory of the leak-rate of seals’, J. Phys.: Condens. Matter, vol. 20, no. 31, p. 315011, Jul. 2008. doi: https://doi.org/10.1088/0953-8984/20/31/315011

[14] B. Lorenz and B. N. J. Persson, ‘Leak rate of seals: Effective-medium theory and comparison with experiment’, Eur. Phys. J. E, vol. 31, no. 2, pp. 159–167, Feb. 2010. doi: https://doi.org/10.1140/epje/i2010-10558-6

[15] F. Bottiglione, G. Carbone, and G. Mantriota, ‘Fluid leakage in seals: An approach based on percolation theory’, Tribol. Int., vol. 42, no. 5, pp. 731–737, May 2009. doi: https://doi.org/10.1016/j.triboint.2008.10.002

[16] M. Scaraggi and B. N. J. Persson, ‘Time-Dependent Fluid Squeeze-Out Between Soft Elastic Solids with Randomly Rough Surfaces’, Tribol. Lett., vol. 47, no. 3, pp. 409–416, Jun. 2012. doi: https://doi.org/10.1007/s11249-012-9996-6

[17] C. Peng, F. Fischer, K. Schmitz, and Hubertus Murrenhoff, ‘Comparative analysis of leakage calculations for metallic seals of ball-seat valves using the multi-asperity model and the magnification-based model’, Tribol. Int., vol. 163, pp. 107130–107130, Nov. 2021. doi: https://doi.org/10.1016/j.triboint.2021.107130

[18] F. Pérez-Ràfols and A. Almqvist, ‘Generating randomly rough surfaces with given height probability distribution and power spectrum’, Tribol. Int., vol. 131, pp. 591–604, Mar. 2019. doi: https://doi.org/10.1016/j.triboint.2018.11.020

[19] Y. Wang and Y. Liu, ‘Preparation of measured engineering surfaces for modeling tribological systems, part I: Characterization and reconstruction’, Tribol. Int., vol. 199, pp. 110026–110026, Jul. 2024. doi: https://doi.org/10.1016/j.triboint.2024.110026

[20] T. D. B. Jacobs, T. Junge, and L. Pastewka, ‘Quantitative characterization of surface topography using spectral analysis’, Surf. Topogr.: Metrol. Prop., vol. 5, no. 1, pp. 013001, Jan. 2017. doi: https://doi.org/10.1088/2051-672x/aa51f8

[21] N. L. Johnson, ‘Systems of Frequency Curves Generated by Methods of Translation’, Biometrika, vol. 36, no. 1/2, p. 149, Jun. 1949. doi: https://doi.org/10.2307/2332539

[22] Tatsunori Tomota, Yasuhiro Kondoh, and Toshihide Ohmori, ‘Modeling Solid Contact between Smooth and Rough Surfaces with Non-Gaussian Distributions’, Tribol. Trans., vol. 62, no. 4, pp. 580–591, Apr. 2019. doi: https://doi.org/10.1080/10402004.2019.1573341

[23] J. Wang, J. Li, N. Bauer, and K. Schmitz, ‘Numerical study of leakage rate in reciprocating seal with non-Gaussian topography characteristics using percolation mechanism’, Tribol. Int., vol. 199, p. 109955, Nov. 2024. doi: https://doi.org/10.1016/j.triboint.2024.109955

Biographies

Jiehao Wang received the bachelor's degree in mechanical design, manufacturing and automation from Shanghai University of Engineering Science in 2017, the master's degree in mechatronic engineering from University of Shanghai for Science and Technology in 2020. He is currently a Ph.D. candidate majoring in mechatronic engineering at Tongji University. His research areas include seals, friction and wear and surface topography.